In situ Scanning Tunneling Microscopy of Ni(100) in 1 M NaOH

Sheuh-Lin Yau, Fu-Ren F. Fan, Thomas P. Moffat, and Allen J. Bard

More About This Article

The permalink http://dx.doi.org/10.1021/j100072a016 provides access to:

- Links to articles and content related to this article
- Copyright permission to reproduce figures and/or text from this article

In Situ Scanning Tunneling Microscopy of Ni(100) in 1 M NaOH

Sheuh-Lin Yau, Fu-Ren F. Fan, Thomas P. Moffat,[†] and Allen J. Bard[*]

Department of Chemistry and Biochemistry, The University of Texas at Austin, Austin, Texas 78712

Received: November 9, 1993; In Final Form: March 30, 1994[⊕]

In situ scanning tunneling microscopy (STM) was used to study anodically grown oxide on Ni(100) and on polycrystalline Ni in 1 M NaOH. Oxidation at low potentials (–0.7 to –0.5 V vs NHE) resulted in a well-ordered rhombic structure which has not been previously identified. This structure was resistant to reduction, which suggests that it is intimately linked to the irreversible nature of the Ni/Ni(OH)$_2$ voltammetric peak. As the potential was increased through the passive regime, the rhombic structure became distorted, and, at higher potentials (>0.18 V vs NHE), a quasi-hexagonal structure was observed with a nearest-neighbor spacing consistent with either β-Ni(OH)$_2$(0001) or NiO(111). In the transpassive regime, ~0.6 V, the hexagonal structure was largely unaltered by the Ni(OH)$_2$/NiOOH reaction. This is consistent with the proposed one-electron oxidative deprotonation/proton insertion mechanism. However, if the potential sweep was extended to 0.8 V, an additional modulation of the electron density occurred with a characteristic length of 1.5–2.0 nm.

Introduction

The oxide films produced by anodic oxidation of nickel play a central role in a variety of electrochemical technologies ranging from passivation to electrocatalysis.[1-5] The excellent corrosion resistance of nickel in alkaline media is attributed to the formation of either a Ni(OH)$_2$[6,7] or a NiO/Ni(OH)$_2$[8-10] bilayer film. The further oxidation of the Ni(II)-based overlayer to a NiOOH-type film is the basis of the Ni(II,III) battery electrode[1] and related electrochromic devices.[4] Extensive studies of nickel in alkaline solution demonstrate that the precise nature of the oxide film is a marked function of the electrochemical history of the electrode.[7,11,12] Yet, despite numerous spectroelectrochemical investigations,[6,7,12] many details concerning the composition and structure of the oxides, as well as the dynamics of formation and reduction, remain to be resolved. Recently, scanning tunneling microscopy (STM) has been used to examine the passive film formed on nickel.[13,14] In this paper, we address the issue of oxide film structure by presenting the first atomic resolution in situ STM observations of the (100) nickel electrode passivated in 1 M NaOH under potential control. These observations are supplemented by similar results for polycrystalline nickel.

Experimental Section

All STM and voltammetric measurements were performed in a quiescent 1 M NaOH solution prepared from reagent grade NaOH (Fisher Scientific) and Millipore water (>18-MΩ resistivity). A (100) oriented Ni single crystal and mechanically-rolled polycrystalline Ni were obtained from Johnson-Matthey (Ward Hill, MA). Laue back-diffraction was performed to verify the orientation of the (100) crystal. The crystal was tilted with the (100) axis deviating 2° from the surface normal in the [010] direction. The orientation of the (100) crystal with respect to the x- and y-axes of the scanning tunneling microscope is shown in Figure 1. The crystal surface was polished with an alumina–water slurry to a ~0.05-μm-diameter γ-Al$_2$O$_3$ particle finish. After being sonicated in acetone and Millipore water for 10 min, the Ni(100) electrode was rinsed thoroughly with Millipore water. While the surface largely had a mirror finish, a few polishing scratches were still visible. A warm (ca. 50 °C) solution of 10 mL of H$_3$PO$_4$, 30 mL of HNO$_3$, 10 mL of H$_2$SO$_4$, and 50 mL
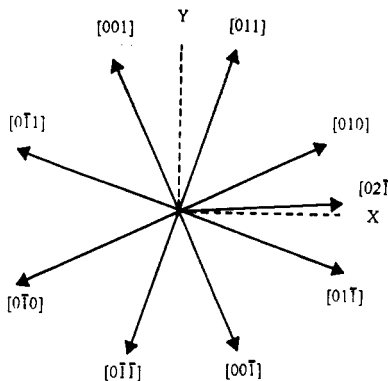

Figure 1. Orientation of the Ni(100) single crystal surface with respect to the STM scan directions.

of CH$_3$COOH was used to etch the Ni(100) electrode to remove the polishing damage.[11] The polycrystalline nickel electrode was used immediately after mechanical polishing. After etching or mechanical polishing, the electrodes were transferred to the STM electrochemical cell. The (100) Ni electrode was activated by sweeping the potential into the hydrogen discharge region at 50 mV/s to –1.3 V vs NHE, where it was held for 30 s. According to the literature,[6,7,11] this reduction procedure results in removal of the air-formed oxide. Cyclic voltammetry was performed by sweeping the potential in the positive direction at 50 mV/s. For the Ni(100) STM experiment, a similar specimen preparation procedure was followed except potential control was interrupted following the reduction step. Upon releasing potentiostatic control, the electrode settled at a value of –0.7 V vs NHE, which is in the region of the first anodic voltammetric wave. This shift in potential was presumably the result of oxygen reduction since the electrolytic cell was exposed to the atmosphere.

The STM experiments were performed using a commercially available instrument (Nanoscope II, Digital Instruments, Santa Barbara, CA). The in situ STM electrochemical cell was a standard commercial cell, described elsewhere.[15] The STM tip electrodes were produced by electrochemically etching tungsten wire (0.01 in.; FHD Metals, Brunswick, NE) in 1 M NaOH at 12-V ac, with respect to a carbon electrode serving as a counter electrode. The tips were then thoroughly rinsed with Millipore water, dried with acetone, and insulated with transparent nail polish (Wet 'n Wild, Pavion Ltd., Nyack, NY).[13] The coated W tips were allowed to dry for at least 10 min before performing the in situ STM experiments. Approximately 80% of the time
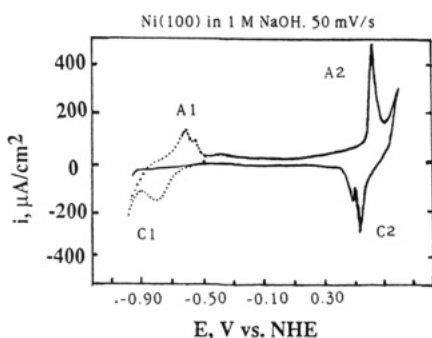

Figure 2. Cyclic voltammogram of a Ni(100) electrode in 1 M NaOH. The air-formed oxide was reduced at –1.3 V for 30 s before sweeping the potential from –1 V at 50 mV/s. The anodic wave (A1) is followed by a current plateau, the Ni^{2+}/Ni^{3+} oxidation (A2) at +0.60 V, and oxygen evolution at +0.8 V. The cathodic scan contains a reduction wave (C2) for the Ni^{2+}/Ni^{3+} couple and a wave (C1) for the reduction of α-Ni-$(OH)_2$ at –0.8 V. The (C1) was shifted toward negative potentials and merged with hydrogen evolution once the upper potential limit became more positive than –0.4 V.

this procedure generated tips that could achieve atomic resolution in solution. Two platinum wires served as the quasi-reference and counter electrodes, respectively. All reported potentials refer to the normal hydrogen electrode (NHE). This correction was accomplished by comparing the potentials of well-defined Ni waves to previously reported data.[8]

Results

Cyclic Voltammetry of Ni(100) in 1 M NaOH. A cyclic voltammogram (CV) for Ni(100) in 1 M NaOH is shown in Figure 2. This was obtained by sweeping the potential positively from –1.0 V at 50 mV/s. The CV is in good agreement with previous observations,[6–8] indicating that the chemical etching pretreatment did not strongly affect the surface chemistry. The anodic sweep contains a broad wave at –0.6 V (A1), followed by a current plateau spanning more than 1 V. The A1 wave is typically attributed to the formation of a monolayer of α-Ni-$(OH)_2$.[1,6,7,11] Close inspection reveals that the wave is actually composed of at least two processes. As noted by others, hydrogen desorption and other related processes may contribute to A1.[11,16,17] In fact, earlier work suggested that nickel is not stable in argon-deaerated solutions due to proton reduction or adsorption.[1,6,7,12] Reversing the sweep direction at –0.5 V yields a cathodic wave at –0.8 V (C1), which has been associated with the reduction of α-Ni$(OH)_2$.[1,6,7] However, once the upper potential limit exceeded –0.4 V, the C1 feature merged with H_2 generation and A1 disappeared during subsequent scans. The attenuation of C1 has been ascribed to the irreversible dehydration of α-Ni$(OH)_2$ to β-Ni$(OH)_2$ when the potential is increased past –0.4 V.[1,6,7] A similar effect was observed if an activated Ni(100) electrode (prebiased at –1.3 V vs NHE for ca. 30 s) was aged at rest potential for several minutes. However, the A1 wave could be retrieved by sweeping the potential to values more negative than –1 V. Nevertheless, the recovered A1 feature was broader than that in the first sweep. This has been correlated to increasing disorder of the surface.[11] As the potential is increased beyond –0.4 V, the voltammetric current is constant at ~50 $\mu A/cm^2$ for ca. 1 V. This corresponds to the growth of approximately three layers of β-Ni$(OH)_2$.[7] However, both ellipsometric[10] and second-harmonic generation[12] experiments demonstrate that changes in addition to film thickening occur in this range. A modulated photoreflectance[9] and an X-ray photoelectron[8] study suggest that the film is a bilayer of NiO and Ni$(OH)_2$. As the potential is increased further, a sharp anodic voltammetric peak emerges at +0.64 V (A2) due to the conversion of the Ni(II)-based overlayer to a complex higher-valent oxide that is generically referred to here as NiOOH.[1,6,7,12] At potentials greater than +0.70 V, the current
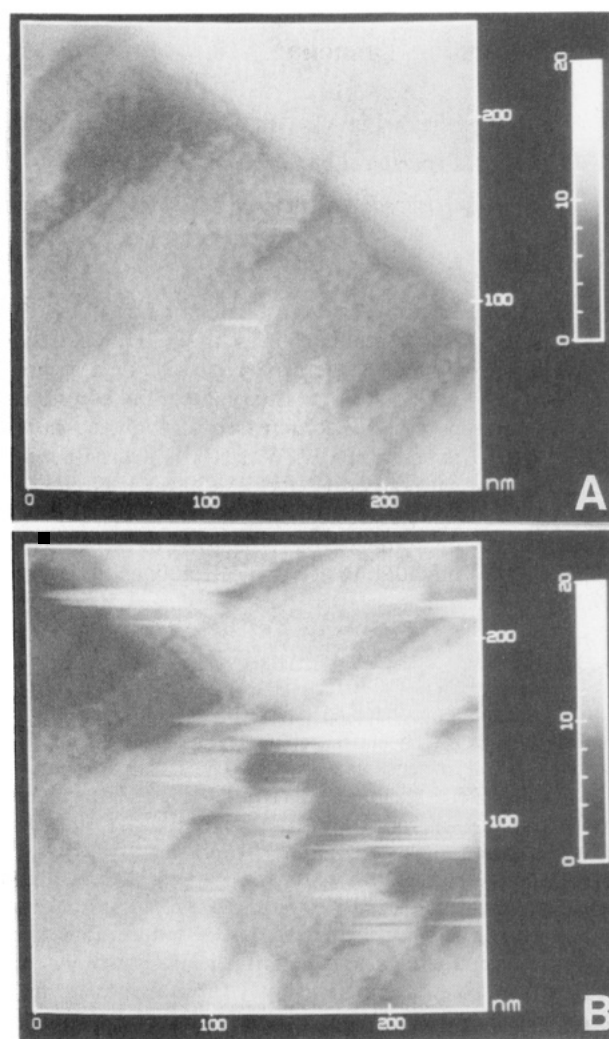

Figure 3. Topographic STM images of polycrystalline Ni during repetitive stepping of the potential between hydrogen evolution and the passive region. The images were obtained at (A) –0.77 V and (B) –0.90 V. The tip potential was held at –0.45 V and the set-point current was 2 nA. The step height between terraces occurs as integers of 0.5 nm.

increases rapidly with O_2 evolution. The reverse scan includes a doublet peak (C2) corresponding to the reduction of Ni-OOH.[1,6,7,12] This is followed by a featureless region spanning 1 V, while a rapid increase of current commences at –0.90 V due to water reduction.

STM Atomic Resolution of Passivated Ni(100). Initially, several attempts were made to image freshly polished Ni(100) in air. However, obtaining stable atomic images proved difficult. Typically, the images were streaked in the direction of the tip raster. This is due to the strong interactions that occur between the STM tip and the thin semiconducting[8] air-formed oxide layer (~1 nm thick) when attempting to maintain a set-point tunneling current. Those tip–film interactions resulted in images that changed with time.

Preliminary in situ experiments were performed with mechanically polished polycrystalline nickel. Stable images of the passivated electrode were routinely observed in 1 M NaOH. However, stepping the potential into the hydrogen evolution region resulted in imaging instabilities as shown in Figure 3. These localized tracking errors are associated with physical or electronic changes that occur at these sites. While the precise nature of the effect is not understood, similar phenomena have been seen for nickel and chromium cycled in sulfuric acid between the passive state and the hydrogen evolution/film reduction region.[18]

In situ experiments with Ni(100) were initiated after the electrode had been reduced at –1.3 V for 30 s followed by releasing

Figure 5. In situ STM image obtained at –0.7 V revealing several terraces with a well-ordered rhombic structure. Note the enhanced electron density at the kink sites on the terrace steps. The tip was biased 180 mV with respect to the Ni electrode and the feedback current was 5 nA.
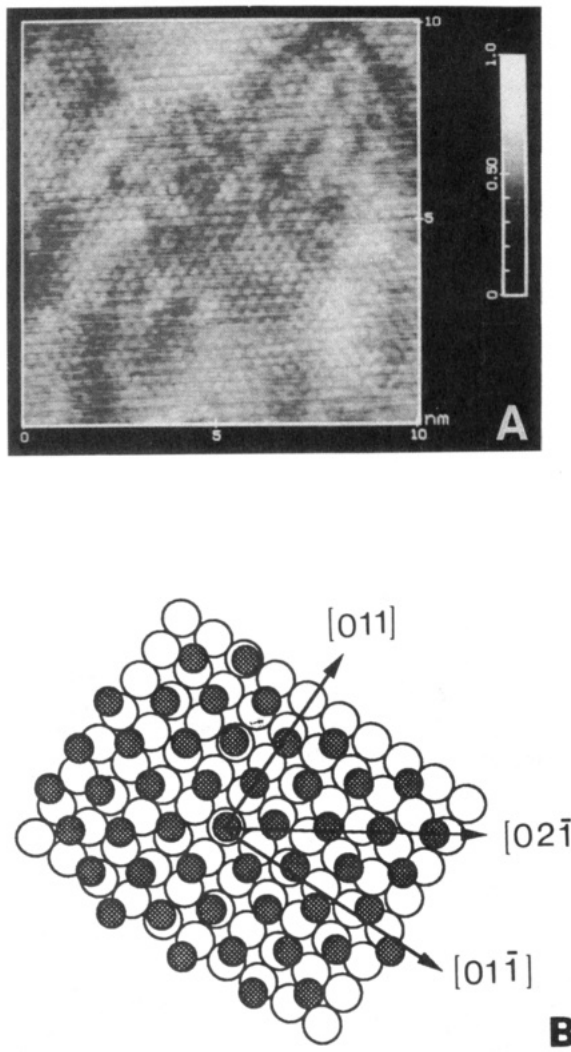

Figure 4. (A) In situ STM image of a hexagonal lattice on a Ni(100) electrode at –1 V after the electrode has been aged at rest potential for several minutes. The tip potential was held at –0.4 V, and the feedback current was set at 5 nA. The 0.32-nm lattice constant corresponds to an 22% expansion from the Ni(100) lattice. An uneven intensity distribution of electron density is apparent, which could be attributed to registry variation between the Ni^{2+} layer and the substrate. (B) Ball model for the (0001) plane of $Ni(OH)_2$ on a Ni(100) substrate. The filled circles arranged in a hexagonal pattern represent the Ni^{2+} array in $Ni(OH)_2$.

potential control. The electrode floated at ca. –0.7 V for several minutes. Both IR[6] and UV–vis[7] reflectance studies indicate that the film-free surface of Ni is unstable upon immersion in NaOH. According to the voltammetric results, nickel is oxidized to Ni-$(OH)_2$ at this potential. Initially, an attempt was made to image film-free Ni(001) by reducing the surface at very negative potentials. However, imaging instabilities like those noted for polycrystalline nickel occurred. Consequently, the first atomic-resolution images were obtained at –1 V after the electrode had been aged at the rest potential for several minutes. As shown in Figure 4, a quasi-hexagonal mesh of electron density was observed with a nearest-neighbor spacing of ~0.32 nm. The near 6-fold symmetry and nearest-neighbor spacing suggest that this structure corresponds to the (0001) basal plane of $Ni(OH)_2$ (CdI_2 or C6 structure).[1] Alternatively, if a 10% uncertainty in the length measurement is allowed, this structure may be a remnant of an air-formed (111) NiO passive film. In either case, a ~22% expansion exists between the primitive lattice of Ni(100) and the passivating overlayer. This mismatch gives rise to an additional modulation of the electron density on the order of 1.0 nm.

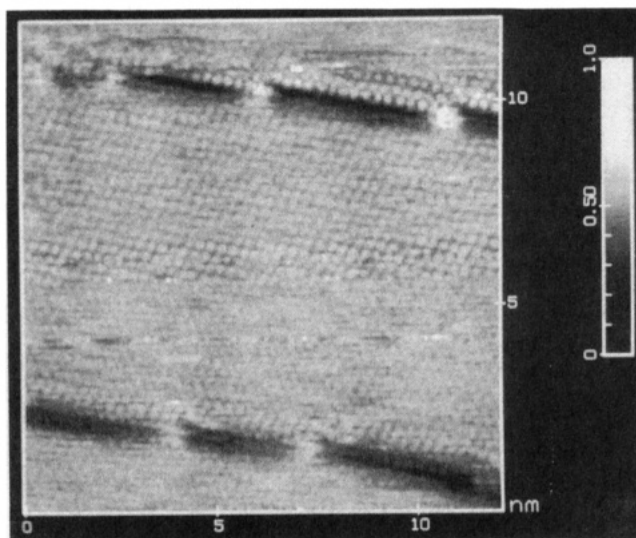When the potential is swept anodically to –0.7 V, a new structure, shown in Figure 5, is observed. Remarkably uniform

packing occurs on the terraces, which can be greater than 5 nm wide and 20 nm long. The terraces are separated by steps 0.44 nm in height. Several kink sites with enhanced electron density are visible on the terrace ledges. A high-resolution unfiltered image of the terrace structure is given in Figure 6. The rhombic packing can be characterized by vectors **a** and **b** which are separated by 72°. The **a** vector corresponds to [011] of the Ni-(100) substrate. The nearest-neighbor spacing is ~0.29 nm. The symmetry and dimensions of the overlayer do not correspond to the known characteristics of α- or β-$Ni(OH)_2$.[1] Similarly, while the nearest-neighbor spacing is close to that of (100) NiO and (111) NiO (0.295 nm), the deviation from cubic and hexagonal symmetry precludes such an identification. No larger scale modulation of the electron density was observed despite the large mismatch between the overlayer and Ni(100). This well-ordered surface structure was quite stable and could not be reduced at –0.9 V. We attribute the irreversible behavior of the A1–C1 voltammetric wave to the growth of this structure.

When the potential is increased further into the passive regime, voltammetric measurements reveal a current plateau which is typically associated with film thickening. However, as noted earlier, ellipsometric[10] and second-harmonic generation[12] studies indicate that substantial changes, beyond simple film growth, occur in this regime. In situ STM provides a direct method for examining this issue. However, as the film thickness increases, physical interactions between the scanning tip and the semiconductive film occur. Nevertheless, a remarkable image was obtained for Ni(100) poised at 0.0 V. As shown in Figure 7, the rhombic structure observed at lower potentials is highly distorted, forming a superstructure with a characteristic cell size on the order of 1.5 nm. It is possible that this structure may be the result of tip–overlayer interactions or tip changes. However, the dimensions and orientation of this cell structure correlate reasonably well with a strained lateral superlattice proposed in the literature for oxidized Ni(100).[19] In this instance, the distortion is a consequence of the large misfit between the lattice parameters of NiO(100) and Ni(100).

As the potential is increased to 0.18 V, the distorted rhombic structure appears to relax toward a close-packed hexagonal structure, as shown in Figure 8. The close-packed directions are separated by 64°, as compared to 72° found at lower potentials. The nearest-neighbor spacing was ~0.31 nm, which may correspond to either $Ni(OH)_2(0001)$ (0.31 nm) or NiO(111) (0.295 nm). The terrace step height was 0.45 nm. A closer examination of the image reveals a distribution of nearest-neighbor
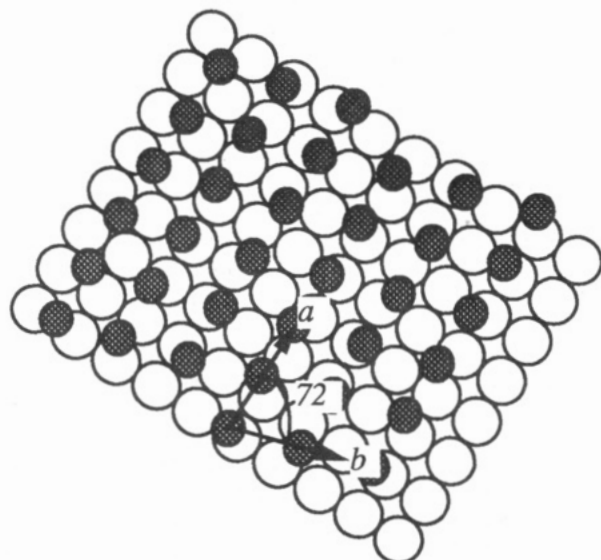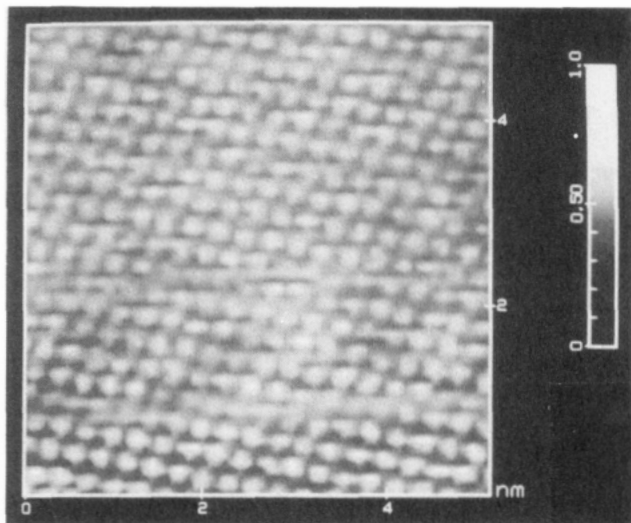
Figure 6. (A) High-resolution image of the rhombic structure on a Ni-(100) electrode held at –0.7 V. The vectors **a** and **b**, which represent the close-packed directions, are separated by a 72° angle, as depicted in B. The nearest-neighbor spacing along **a** and **b** is 0.29 nm. The a vector is parallel to the [011] of the Ni(100) substrate. The image was acquired with a 186-mV bias voltage and 5-nA feedback current. (B) Ball model for the rhombic $Ni(OH)_2$ structure (filled circles) on top of the nickel substrate (open circles).

Figure 7. (A) In situ STM atomic resolution revealing the atomic configuration of the oxide structure on Ni(100) at 0 V. The tip potential was –0.45 V. This image may represent a transition state between the rhombic structure and the quasi-hexagonal lattice. (B) 2D FFT pattern of the image shown in A. The two spots marked by P are attributed to the superstructure with a cell size on the order of 1.5 nm.

spacings. The spacing between neighboring close-packed rows ranged from 0.28 to 0.4 nm. A modulation of the electron density due to changes in registry of the overlayer is superimposed upon that of the individual atomic species.

At higher potentials, ~0.3 V, the hexagonal structure was more clearly defined. As shown in Figure 9, well-ordered regions, ~5.0 × 5.0 nm, were found with a nearest-neighbor spacing of 0.29 nm.

The transpassive, $Ni^{2+/3+}$ battery reaction was examined by sweeping the potential at 50 mV/s to 0.6 V. After holding the potential at 0.6 V, the anodic current density became negligible after ~3 min. A hexagonal structure was observed, as shown in Figure 10, with a nearest-neighbor spacing of 0.29 nm. The packing arrangement and orientation was indistinguishable from that observed at 0.3 V. However, high-resolution images (i.e., less than 30 × 30 nm) obtained at 0.6 V were observed to alternate between the hexagonal structure and an unresolved disordered phase. The alternation continued over many scans with a period of about 1 min. This suggests the disordering is caused by tip-substrate interactions. When the potential was swept back to 0.3
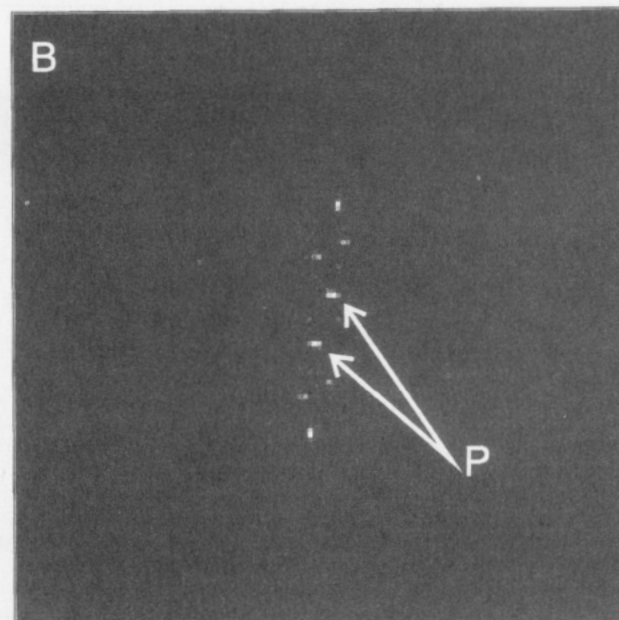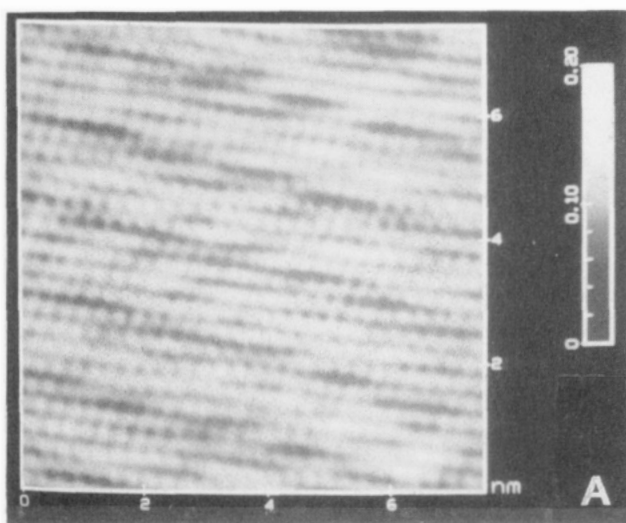
V, the hexagonal structure was retained. However, if the potential scan was extended to 0.8 V, where oxygen evolution occurs, measurable changes in structure were apparent. After several potential cycles between 0.35 and 0.8 V, a stable image was obtained at 0.35 V. As shown in Figure 11, long-range modulation of the electron density was superimposed on the hexagonally packed atomic structure. The hexagonal structure had a nearest-neighbor spacing of 0.29 ± 0.02 nm, while longer range modulation of the electron density yielded ~1.5–2-nm-wide zones of uniform electron density. The close-packed directions were no longer strictly linear and exhibited a wavy character. This may represent an earlier stage in the transformation of β-$Ni(OH)_2$ into a NiOOH nanocrystalline film. Alternatively, this structure may be the result of the change from octahedral symmetry to asymmetric coordination of Ni that accompanies the oxidation of β-$Ni(OH)_2$.[20]

Dynamics of Film Growth and Reduction. In situ STM was used to monitor the growth and reduction of the passivating overlayer. The growth of the rhombic structure was observed
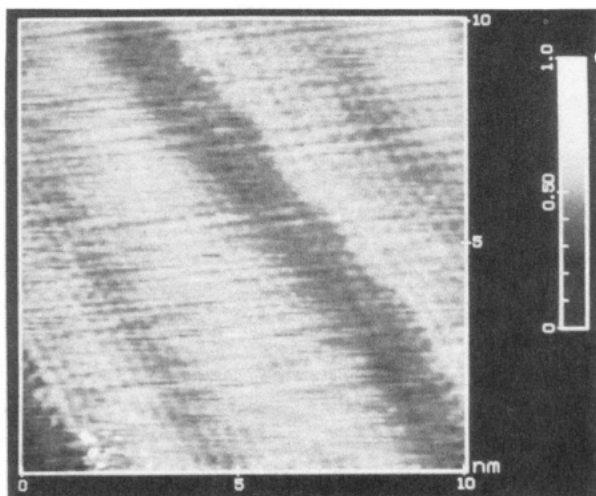
Figure 8. In situ STM atomic resolution of a passive film at 0.18 V showing that the atomic arrangement has become more hexagonal in nature. A close examination reveals a distribution of nearest-neighbor spacings ranging from 0.28 to 0.4 nm.
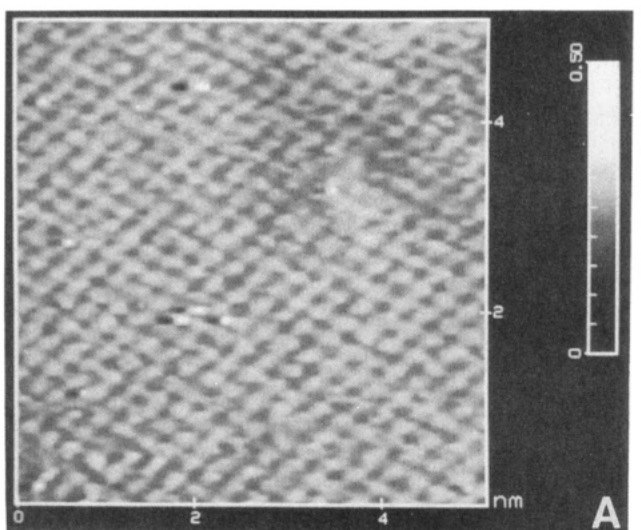

Figure 9. (A) In situ STM image showing the hexagonal structure found on the Ni(100) electrode at 0.35 V. The tip potential was held at −0.45 V. The nearest-neighbor spacing is about 0.29 nm; one close-packed direction of the oxide is parallel to the [01$\bar{1}$] of the Ni(100) substrate. (B) Schematic cross-section of the stacking sequence of oxide on Ni(100) in the [110] direction. The actual film thickness is larger than the monolayers implied by this representation.

while sweeping the potential in the positive direction. Increasing the potential results in significant disruption of the surface order followed by rapid reordering. In Figure 12, the tip was rastered from the bottom toward the top, while the potential was swept from −0.7 to −0.5 V at 50 mV/s. Initially, the structure was unaltered, but with increasing overpotential, a large corrugated perturbation developed with a wavelength of roughly 1.2 nm. This large-scale modulation is likely the result of convolution of the instrumental response with imaging instabilities induced by the film growth process. Closer examination of this image reveals small ordered regions beneath the overlaying perturbations. Whether this is an intermediate structure or represents another layer of the growing oxide film remains to be resolved. With time, this disturbed region proceeds to relax toward the well-
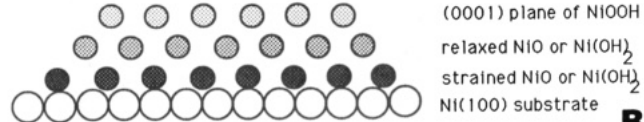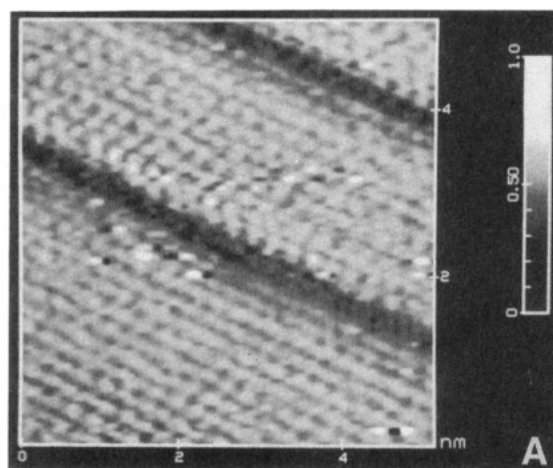

Figure 10. (A) In situ STM image of the Ni(100) electrode at 0.6 V. The tip electrode was poised at −0.45 V. The image reveals the hexagonal pattern of electron density with nearest-neighbor separation of 0.29 nm. (B) Schematic cross-section of the layered oxide structure. The STM image is believed to represent the (0001) plane of NiOOH whose lattice constant is ca. 10% shorter than that of Ni(OH)$_2$ but roughly the same as that of NiO. Consequently, the long-range hexagonal packing of the Ni(II) lattice is not disrupted by oxidative deprotonation to Ni(III). The actual thicknesses of the oxide layers are larger than the monolayers depicted in this representation.

ordered rhombic structure. The ordered rhombic region shown in the lower portion of this figure is rotated 90° relative to that shown in Figure 4 and thus represents an alternative domain orientation.

A remarkable series of film growth images was obtained for a similar experiment performed with a polycrystalline nickel specimen. In this instance, the first image shown in Figure 13 was obtained after stepping the potential of a passivated electrode (−0.2 V) into the hydrogen evolution region (−0.98 V), where a variety of structures was observed. The top of the image given in Figure 13A is substantially disordered, while a reasonably well-defined rhombic structure is observed in the center. A regime of ordered electron density, with close-packed rows separated by ∼0.39 nm, is also apparent at the bottom right corner. The orientation of the rhombic structure relative to that in the lower right corner is identical to that observed in Figure 12. This suggests that we are looking at a (100) textured grain of the polycrystalline Ni specimen. Film growth was observed by stepping the potential to −0.73 V and collecting the images shown in Figure 13B,C. The lateral growth of the well-ordered rhombic structure is apparent.

Discussion

In situ STM has revealed atomically resolved images of the anodically formed oxides on Ni(100). During the initial stage of in situ oxidation a close-packed hexagonal structure was observed with a nearest-neighbor spacing characteristic of (0001) Ni(OH)$_2$. Upon sweeping the potential through the Ni/Ni(OH)$_2$ voltammetric wave, a new, heretofore unknown, rhombic structure develops. Dynamic analysis indicates that at low potentials the structure forms by lateral growth of well-defined terraces. The rhombic structure is resistant to reduction until the potential is below −0.9 V. Thus, formation of the highly ordered rhombic structure is related to the irreversible nature of the Ni/Ni(OH)$_2$
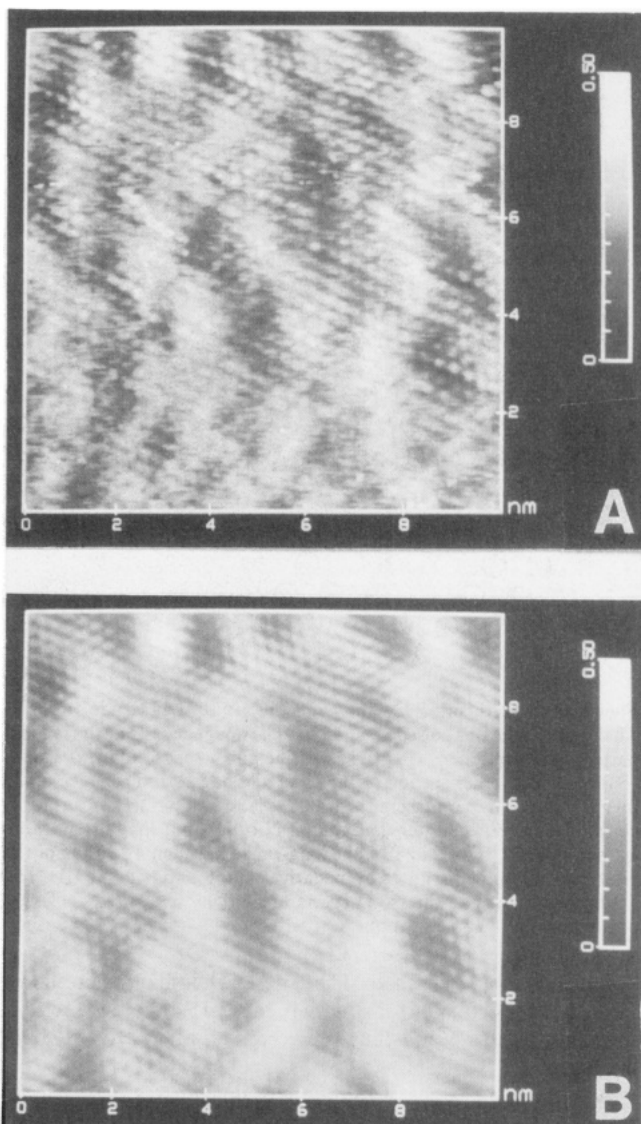
Figure 11. In situ STM image showing the modulated hexagonal lattice of the oxide grown on Ni(100) by cycling the potential between 0.35 and 0.8 V: (A) raw data and (B) filtered image. The image was collected at 0.35 V.

Figure 12. In situ STM image showing disruption of the rhombic lattice during film growth. The Ni potential was swept from –0.7 to –0.5 V, while the image was collected by rastering the tip from the bottom toward the top. The tip potential was set at –0.4 V.

voltammetric wave. Previously, this irreversibility was linked to dehydration of α-Ni(OH)$_2$ forming β-Ni(OH)$_2$.[1,7] However, the symmetry of the rhombic structure is inconsistant with β-Ni-(OH)$_2$ as well as NiO (a NaCl structure).[22-23] The electron density distribution is expected to correlate to atomic positions, although it remains to be resolved whether the rhombic coordinates are for divalent nickel oxide or hydroxide species. According to an XPS study[8] the anodic feature at –0.56 V represents the growth of a four-layer oxide, although earlier coulometric data indicated a two-layer growth at the end of formation of this feature.[7,11] Surprisingly, this film, which exhibits a 22% misfit with the primitive lattice of Ni(100), does not exhibit any larger scale modulation of the electron density.[19,21] Presumably the misfit is highly localized to the metal–film interface and does not perturb the outer layers of the thin film.

As the potential is increased further into the passive range, the structure of the film changes. In some instances, the film develops a quasi-periodic cell structure with a characteristic dimension of 1.5 nm. As noted earlier, this is similar to the strained lateral superlattice proposed for the NiO(100) overlayer formed by exposure of Ni(100) to oxygen at room temperature.[19] However, tip–film interactions, or a multiple tip, might also account for this image. At higher potentials, the rhombic structure changes to hexagonal form with a nearest-neighbor spacing that may be
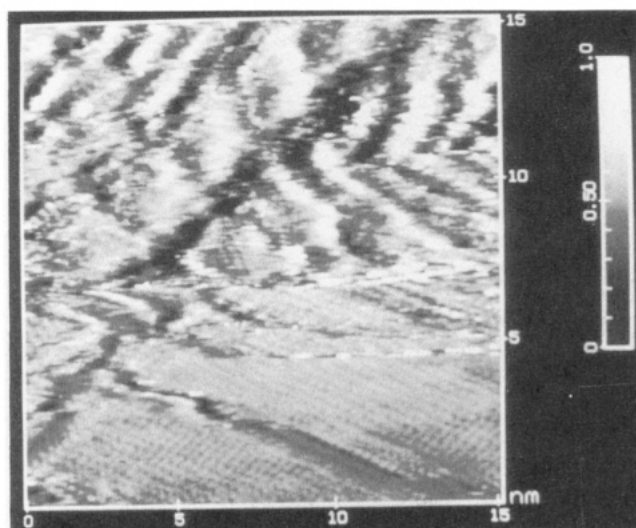
associated with (0001) β-Ni(OH)$_2$[1] or (111) NiO. Interestingly, LEED studies of Ni(100) passivated in perchloric acid indicate the presence of NiO(111) in the passive overlayer.[22] Similar results have been reported from RHEED studies[23] which indicate a 2.5-nm particle size, which is similar to the modulation shown in Figure 11. On electropolished Ni(100), the (111) oxide showed two orientations with respect to the underlying metal. One close-packed direction of the oxide was coincident with that of the substrate. However, the (111) oxide grown by anodization in Na$_2$SO$_4$ was randomly oriented. In our study, the orientational relationship observed was similar to that reported for electropolished nickel.[23] This is shown in Figure 9, where one close-packed direction of the oxide is coincident with [01$\bar{1}$] Ni(100).

The potential independent current of the passive range is often ascribed to thickening of the passive film with increasing potential. Ellipsometry[10] and coulometry[7] give film thickness values ranging from 1.0 to 2.0 nm, while XPS analysis[8] yields values between 1.5 and 4.0 nm. However, second-harmonic generation[12] and ellipsometric[10] measurements indicate that the situation is substantially more complex. The potential dependence of the passive film structure found in this study is in agreement with these optical studies. XPS[8] and reflectance[9] data indicate that the film is a bilayer of NiO/Ni(OH)$_2$ with the inner barrier layer condensing as the film becomes thicker. The preference for (111) NiO over the more stable (100) NiO is explained in terms of the kinetics associated with breaking Ni–Ni bonds in the metal.[21] Similarly, the transformation from hexagonal (0001) Ni(OH)$_2$ to (111) NiO may accordingly be favored. The sensitivity of the oxide film structure to the electrode potential is somewhat analogous to the temperature sensitivity of ultrahigh vacuum grown oxides.[19,21,24] An LEED study[21] during oxidation of Ni-(100) reveals growth of (111) NiO is favored at temperatures below 300 K, while a (7 × 7)-like structure is observed during adsorption between 300 and 400 K. Thus, room temperature represents a crossover point between these two oxide forms.

Variations in synthetic and analytical methods have resulted in much controversy concerning the structure and oxidation state of Ni electrodes at potentials more positive than 0.4 V.[9] The STM results in Figures 10 and 11 reveal a long-range ordered structure which indicates that NiOOH can be of high crystallinity, at least for the experimental conditions used in this study. These results are supportive of the proposed battery reaction of a one-electron oxidative deprotonation (Ni(OH)$_2$ $\rightarrow$ NiOOH + H$^+$ + e$^-$). The hexagonal arrangement, as revealed by STM atomic resolution, is consistent with the previously suggested brucite
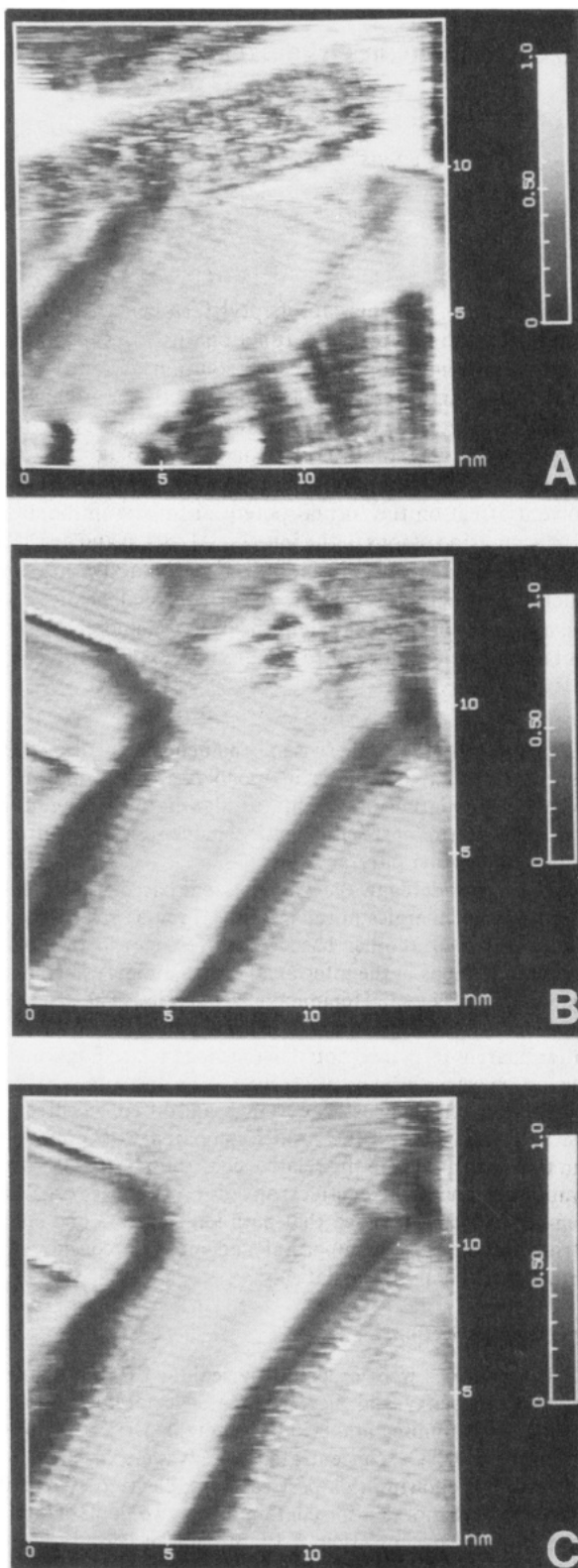
Figure 13. Sequential images of the growth of the oxide film on polycrystalline Ni. The observed rhombic structure suggests that a (001) Ni grain is being imaged. The sequence of images represent the same area, as demarked by the terrace steps. The Ni potential was –0.98 V in A, and succeeding images were collected after stepping the potential to –0.73 V. The tip potential was –0.63 V, and the set-point tunneling current was 21 nA.

structure for β-Ni(OH)$_2$ and β-NiOOH.[1] However, it will be challenging to use STM to verify the 10% lateral contraction in dimension between β-Ni(OH)$_2$ and NiOOH as indicated by EXAFS studies.[1b,20] A further limitation of this study is the strong influence of the tip electrode on the potential of the substrate

being imaged. This in combination with mechanical tip–substrate interaction resulted in imaging instability under certain conditions.

Conclusions

In situ STM analysis has been used to examine the anodic oxides formed on Ni(100) under potential control in 1 M NaOH. A variety of atomically resolved structures have been revealed. At low potentials, a well-ordered rhombic structure was observed which does not correspond to the known structure ascribed to Ni(OH)$_2$ or NiO. The growth of this lattice is responsible for the irreversibility of the Ni/Ni(OH)$_2$ voltammetric wave. At higher potentials in the passive regions, this structure transforms to a hexagonal structure which may correspond to either β-Ni-(OH)$_2$ or NiO(111). As the potential was increased further, this structure was largely unaltered by the β-Ni(OH)$_2$/NiOOH reaction. This is consistent with the one-electron oxidative deprotonation reaction mechanism. Extended cycling of the potential in this regime resulted in a cell structure of $\sim$2.0 nm being superimposed upon the hexagonal lattice.

References and Notes

(1) (a) Avria, A. J.; Posada, D. In *Encyclopedia of the Electrochemistry of Elements*; Bard, A. J., Ed.; Marcel Dekker: New York, 1975; Vol. VIII. (b) McBreen, J. In *Modern Aspects of Electrochemistry*; White, R. E., Bockris, J. O'M., Conway, B. E., Eds.; Plenum Press: New York, 1990; Vol. 21.

(2) *Passivity of Metals and Semiconductors*; Froment, M., Ed.; Elsevier: Amsterdam, 1983.

(3) Sato, N. *Corros. Sci.* **1990**, *31*, 1.

(4) Lampert, C. M.; Omstead, T. R.; Yu, T. *Proc. S.P.I.E.-Int. Soc. Opt. Eng.* **1985**, *562*, 15.

(5) Kinoshita, K. *Electrochemical Oxygen Technology*; Wiley: New York, 1992.

(6) Beden, B.; Bewick, A. *Electrochim. Acta* **1988**, *33*, 1695.

(7) Hahn, F.; Beden, B.; Croissant, M. J.; Lamy, C. *Electrochim. Acta* **1986**, *31*, 335.

(8) Hoppe, H.-W.; Strehblow, H. H. *Surf. Interface Anal.* **1989**, *14*, 121.

(9) Larramona, G.; Gutierrez, C. J. *Electrochem. Soc.* **1990**, *137*, 428.

(10) Paik, W.; Szklarska-Smialowska, Z. *Surf. Sci.* **1980**, *96*, 401.

(11) Weininger, J. L.; Breiter, M. W. *J. Electrochem. Soc.* **1963**, *101*, 484.

(12) Biwer, B. M.; Pellin, M. J.; Schauer, M. W.; Gruen, D. M. *Surf. Interface Anal.* **1989**, *14*, 635.

(13) Baumer, M.; Cappus, D.; Kuhlenbeck, H.; Freund, H.-J.; Wilhelmi, G.; Brodde, A.; Neddermeyer, H. *Surf. Sci.* **1991**, *253*, 116.

(14) Maurice, V.; Talah, H.; Marcus, P. *Surf. Sci.* **1993**, *284*, L341.

(15) Yau, S.-L.; Gao, X. P.; Chang, S. C.; Schardt, B. C.; Weaver, M. J. *J. Am. Chem. Soc.* **1991**, *113*, 6049.

(16) Burke, L. D.; Twomey, T. A. M. *J. Electroanal. Chem.* **1984**, *162*, 101.

(17) Visscher, W.; Barendrecht, E. *J. Appl. Electrochem.* **1980**, *10*, 269.

(18) Moffat, T. P.; Fan, F.-R. F.; Yau, S.-L.; Bard, A. J. Unpublished results.

(19) Saiki, R. S.; Kaduwela, A. P.; Osterwalder, J.; Fadley, C. S.; Brundle, C. R. *Phys. Rev. B* **1989**, *40*, 1586.

(20) Pandya, K. I.; Hoffman, R. W.; McBreen, J.; O'Grady, W. E. *J. Electrochem. Soc.* **1990**, *137*, 383.

(21) Wang, W. D.; Wu, N. J.; Thiel, P. A. *J. Chem. Phys.* **1990**, *92*, 2025.

(22) Wagner, F. T.; Moylan, T. E. *J. Electrochem. Soc.* **1989**, *136*, 2498.

(23) MacDougall, B.; Cohen, M. In *Passivity of Metals*; Frankenthal, R. P., Kruger, J., Eds.; The Electrochemical Society: Pennington, NJ, 1978; p 827.

(24) Brundle, C. R.; Broughton, J. Q. In *The Chemical Physics of Solid Surfaces and Heterogeneous Catalysis*; King, D. A., Woodruff, D. P., Eds.; Elsevier: New York, 1991; Vol. 3A.